Halide alloying and role of central atom on the structural and optical properties of decylammonium germanium 2D perovskites

Rossella Chiara [ID] ; Gianluca Accorsi [ID] ; Andrea Listorti; Mauro Coduri [ID] ; Clarissa Coccia; Costanza Tedesco; Marta Morana [ID] ; Lorenzo Malavasi [✉] [ID]

Check for updates

View Online Export Citation CrossMark

AIP Publishing

Halide alloying and role of central atom on the structural and optical properties of decylammonium germanium 2D perovskites

View Online   Export Citation   CrossMark

Rossella Chiara,[1] (iD) Gianluca Accorsi,[2] (iD) Andrea Listorti,[3] Mauro Coduri,[1] (iD) Clarissa Coccia,[1]
Costanza Tedesco,[1] Marta Morana,[4] (iD) and Lorenzo Malavasi[1,a] (iD)

AFFILIATIONS

[1] Department of Chemistry and INSTM, Viale Taramelli 16, 27100 Pavia, Italy
[2] CNR Nanotec, Institute of Nanotechnology, c/o Campus Ecotekne, via Monteroni, 73100 Lecce, Italy
[3] Department of Chemistry, University of Bari "Aldo Moro", Via Orabona 4, 70126 Bari, Italy
[4] Department of Earth Sciences, University of Firenze, Via G. la Pira 4, 50121 Firenze, Italy

[a] Author to whom correspondence should be addressed: lorenzo.malavasi@unipv.it. Tel.: +39 382 987921

ABSTRACT

We report here a novel series of halide alloyed Ge-containing 2D perovskites including decylammonium as organic spacer, namely $DA_2Ge(Br_{1-x}I_x)_4$. This system forms a continuous solid solution on the halide site with a modulation of the bandgap from 2.74 to 2.17 eV with a rapid decrease up to $x = 0.5$ followed by a plateau. Iodide-rich compositions show enhanced broad room temperature (RT) photoluminescence (PL) that narrows at low temperature with maximum quantum yields for mixed compositions. The replacement of Ge with Pb and Sn in DA_2GeBr_4 and DA_2GeI_4 provides a tuning of the bandgap in the whole visible spectrum with a marked blue-shift when lead is present and, opposite, a red-shift for Sn replacement. The RT PL progressively broadens moving from Pb to Sn and to Ge covering an emission range from 400 to 800 nm. Finally, the air stability of lead-free 2D perovskites of this work has been determined indicating its improvement by increasing the hardness of the halide.

INTRODUCTION

2D metal halide perovskites (MHPs) are widely investigated for their possible applications in several fields ranging from photovoltaics and photodetection to photocatalysis.[1–6] From a structural point of view, both Ruddlesden–Popper (RP) and Dion–Jacobson (DJ) families, of general formula $A'_2A_{n-1}M_nX_{3n+1}$ and $A'A_{n-1}M_nX_{3n+1}$, respectively (where A' and A = organic cations and n = number of staggered inorganic layers made of metal M and halide X), can be seen as composed by inorganic slabs with octahedrally coordinated metal ions (usually Pb), separated by ammonium organic ligands coordinated to the halides of the octahedra.[1] One of the most appealing characteristics of 2D MHPs is their vast chemical (and in turn structural) tunability that can be modulated by changing the organic spacer, the central atom, and the halide.[1] The database of the actually known 2D perovskites can be found in Ref. 7.

Lead-based 2D perovskites reported so far are close to 700 compositions, followed by tin (79) and finally germanium (2). On the other hand, the recent interest in exploring novel lead-free phases, triggered by the high toxicity of lead, which will strongly limit the real use of any material containing this element, requires to significantly expand the plethora of lead-free 2D perovskites.[8–10] In this context, tin based materials, as mentioned earlier, have received significant attention in recent years, being this element a quite straightforward alternative to lead based on its electronic structure. However, Ge-containing 2D or even 3D perovskites have been very scarcely considered in the current literature even though some encouraging and interesting properties have been demonstrated in several applicative fields.[6,11–16] Such lack of investigation strongly limits the establishment of solid structure–property correlation in Ge-based perovskites, which is a pre-requisite to design optimized and novel materials. We recently tried to fill this gap by computationally and

28 June 2023 08:33:29

experimentally exploring a series of germanium 2D MHPs, including aromatic monoammonium cations, clarifying the role of different structural distortion parameters on the optical properties.[16] Such work allowed us, for example, to further design air and water stable 2D Ge perovskites for photocatalytic applications or to modulate a broad-band emission through external pressure application.[6,17] In order to provide new compositions and understanding the role of metal nature and halide alloying on the structural and optical properties of low-dimensional perovskites, we report here the investigation of a novel series of 2D Ge-containing MHPs, including decylammonium (DA) as organic spacer.

We started our investigation by exploring the role of halide alloying on the $DA_2Ge(Br_{1-x}I_x)_4$ solid solution with $x = 0$, 0.15, 0.25, 0.50, 0.75, 0.85, and 1. Concerning the two end-members, DA_2GeI_4 has been reported previously by our group in a high-pressure diffraction and spectroscopy work, while DA_2GeBr_4, as well as the mixed compositions, have, to the best of our knowledge, never been reported before.[17] $DA_2Ge(Br_{1-x}I_x)_4$ samples were prepared by solution chemistry, and a picture of the obtained powders is reported in Fig. 1(a). As can be seen, sample color moves from light-yellow for $x = 0$ to dark orange for $x = 1$. The room temperature (RT) x-ray diffraction (XRD) patterns [Figs. 1(b) and 1(c)] have the clear features of RP 2D perovskites, with low-angle peaks related to the

long c-axis, and are in agreement with our previous results confirming an orthorhombic symmetry (space group $Pbca$) for the whole the solid solution.[17] All the patterns are strongly dominated by the (00l) reflections typical of the layered perovskites. From Fig. 1(c), highlighting the first peak of the patterns, it is evident a sudden change of the c-axis between $x = 0.25$ and $x = 0.5$. The c-axis is longer for DA_2GeBr_4 and Br-rich compositions with respect to DA_2GeI_4 (and I-rich compositions). Such a trend has been already observed by our group in tin-based systems with aliphatic spacers and is related to the staggering of the organic spacer.[18] The evolution of the c-axis as a function of x (iodide content) is presented in Fig. 1(d); before and after the jump, the slight change of the long axis is due to the different size of the Br and I anions.

UV-vis spectroscopy spectra for the $DA_2Ge(Br_{1-x}I_x)_4$ system are reported in Fig. 2(a). They show well-defined absorption edges that red shift with the increase in iodide amount (x), as further confirmed by the trend of the bandgap calculated from the Tauc plots (reported in the supplementary material, Fig. S1) and shown in Fig. 2(b). By increasing the iodide content (x) from DA_2GeBr_4, the bandgap significantly reduces from 2.74 eV ($x = 0$) to about 2.21 for $x = 0.5$. On the other hand, in the range from $x = 0.5$ to $x = 1$, it only moderately decreases from 2.21 to 2.17. The trend in bandgap variation closely resembles the trend of c-axis as a function of x [cfr.
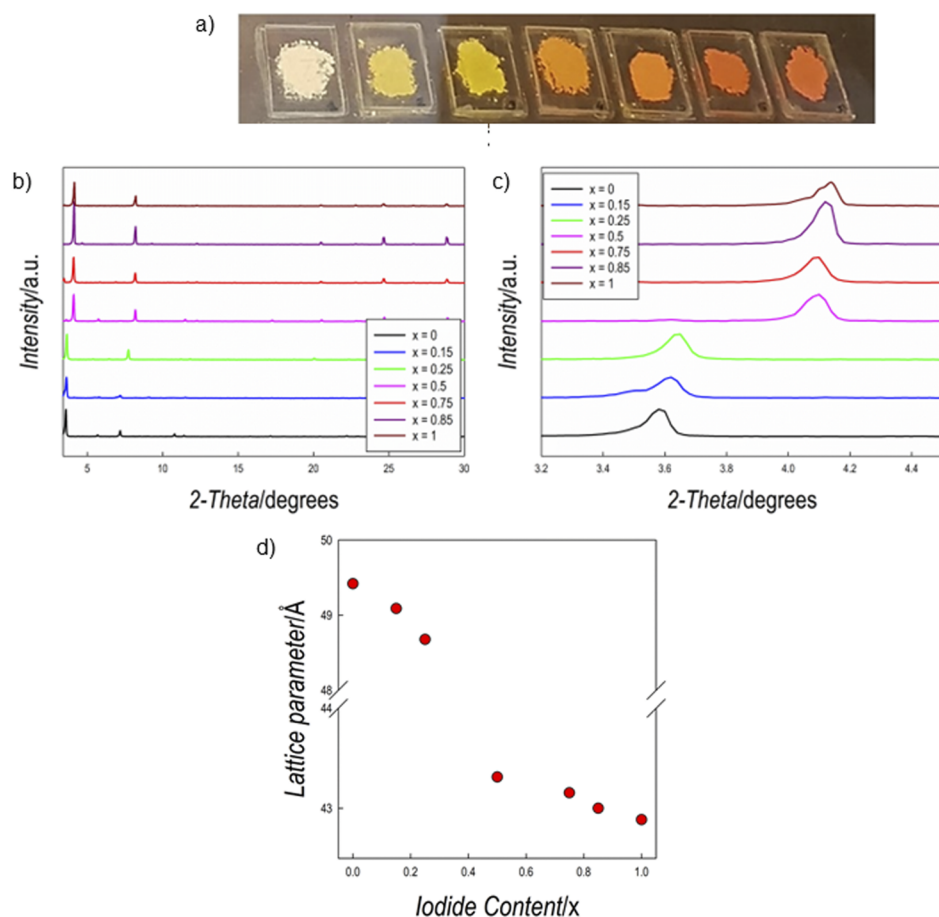

FIG. 1. (a) Pictures of the samples of the $DA_2Ge(Br_{1-x}I_x)_4$ solid solution from $x = 0$ (light yellow on the left) to $x = 1$ (dark orange on the right); (b) XRD patterns of the of the $DA_2Ge(Br_{1-x}I_x)_4$ solid solution; (c) enlargement of the first XRD peak of (b); and (d) evolution of the c-axis vs iodide content for the $DA_2Ge(Br_{1-x}I_x)_4$ system.
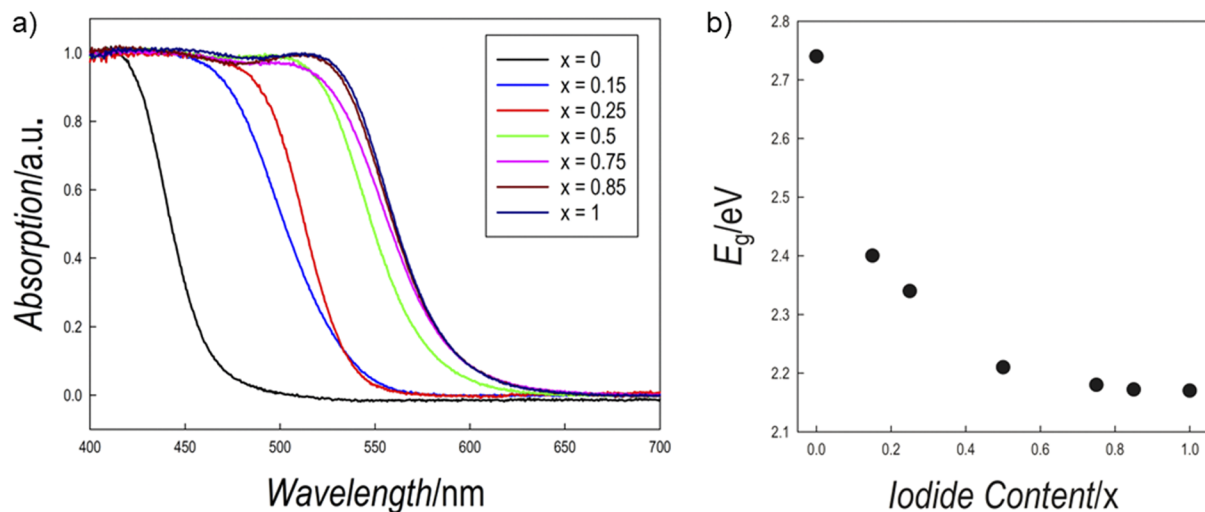
FIG. 2. (a) Absorption spectra of the $DA_2Ge(Br_{1-x}I_x)_4$ system; (b) bandgap variation as a function of the iodide content (x).

Fig. 1(d)], suggesting the central role of the structural parameters in determining the optical edge of these samples.

The photoluminescence (PL) response of the $DA_2Ge(Br_{1-x}I_x)_4$ system is reported in Fig. 3(a). From $x = 0$ to $x = 0.25$, the emission at RT is nearly absent, while from $x = 0.50$ it becomes detectable, and increases as function of the iodide content reaching its maximum for DA_2GeI_4. The emission is very broad and shapeless, it covers most of the visible spectrum (from about 500 to 800 nm), and its feature at RT seems not to be significantly affected by the halide alloying. This broadband emission may be a consequence of the presence of trapping states induced by defects as well as a more pronounced distortion related by the presence of Ge in comparison to 2D Pb-based perovskites.[16,17] The progressive decrease of PL intensity from DA_2GeI_4 to DA_2GeBr_4 well correlates with the lifetimes trend (τ) (Fig. S2) that spans from $\tau = 1.6$ to $\tau \leq 0.2$ ns along with the increase in bromide content in the solid solution.

For some selected samples of the $DA_2Ge(Br_{1-x}I_x)_4$ system, namely, for $x = 0, 0.25, 0.5, 0.75$, and 1, we also carried out low temperature (LT) PL measurements at 77 K. These are reported in Figs. 3(c)–3(g), respectively. For all the samples, the low-temperature PL measurements show intense emission and a different structuring of the bands for the diverse specimens. For DA_2GeBr_4 [Fig. 3(b)], a very broad and continuous emission is observed from about 600 to about 800 nm. For the iodide containing samples, narrowing of the PL with respect to RT data is observed, with an emission peaking in the range of 630–690 nm and extending over a broad region (550–850 nm). A table summarizing the results of the LT PL measurements is reported in the supplementary material (Table S1). Moreover, at low temperature, lifetimes become significantly longer, by the order of μs, with mixed compositions showing higher values with respect to the two end-members. This improvement in the photophysical properties of intermediate compounds is also evident from the quantum yields (QYs) values. The maximum QY is reached by the sample with $x = 0.5$ (38.9%) followed by the one with $x = 0.25$ (34%). The possible origin of the emission intensity recover at low-T is still under investigation,

but we expect an influence of the temperature on the compound distortion degree and, in addition, low temperature would also contribute to reduce thermal activated exciton hopping, with both these phenomena in turn affecting the self-trapping exciton deactivation processes, as recently reported for analogous two-dimensional tin halide perovskites.[19]

To summarize, the investigation of the novel $DA_2Ge(Br_{1-x}I_x)_4$ system revealed: (i) the formation of a continuous solid solution along with halide alloying with orthorhombic symmetry; (ii) the presence of a relevant discontinuity (contraction) in the long c-axis variation passing from Br-rich to I-rich samples; (iii) the variation of the bandgap from about 2.74 eV (DA_2GeBr_4) to 2.17 eV (DA_2GeI_4) with a different slope as a function of x corresponding to the two regimes of c-axis trend; (iv) a very similar RT PL with negligeable emission for Br-rich samples, which progressively increases along with the increase in the I-content; and (v) an enhancement of PL intensity, narrowing of the peaks, and increase in the τ values by reducing the temperature, with mixed compositions showing the highest QYs.

We further extended the present investigation by exploring the role of central atom nature on the properties of DA_2GeBr_4 and DA_2GeI_4. For this purpose, we replaced Ge with Sn and Pb, thus preparing the following four additional 2D perovskites: DA_2SnBr_4, DA_2PbBr_4, DA_2SnI_4, and DA_2PbI_4. Among these samples, only DA_2PbI_4 has been previously reported in Ref. 19 where, however, the sole structure from single-crystal diffraction was documented, without any details about optical properties.[20]

Figure 4 reports a picture showing the samples considered in the following. The first line shows the color change moving from DA_2GeBr_4 (light yellow) to DA_2SnBr_4 (yellow) and DA_2PbBr_4 (white). The second line referring to DA_2GeI_4, as well, shows how Ge replacement with Sn shifts the color to the red while the presence of Pb changes the color from red to orange.

The RT XRD data for the samples (in a reduced angular range to better highlight the differences) are reported in Fig. 5 for the bromide series (left panel) and for the iodide series (right panel). As
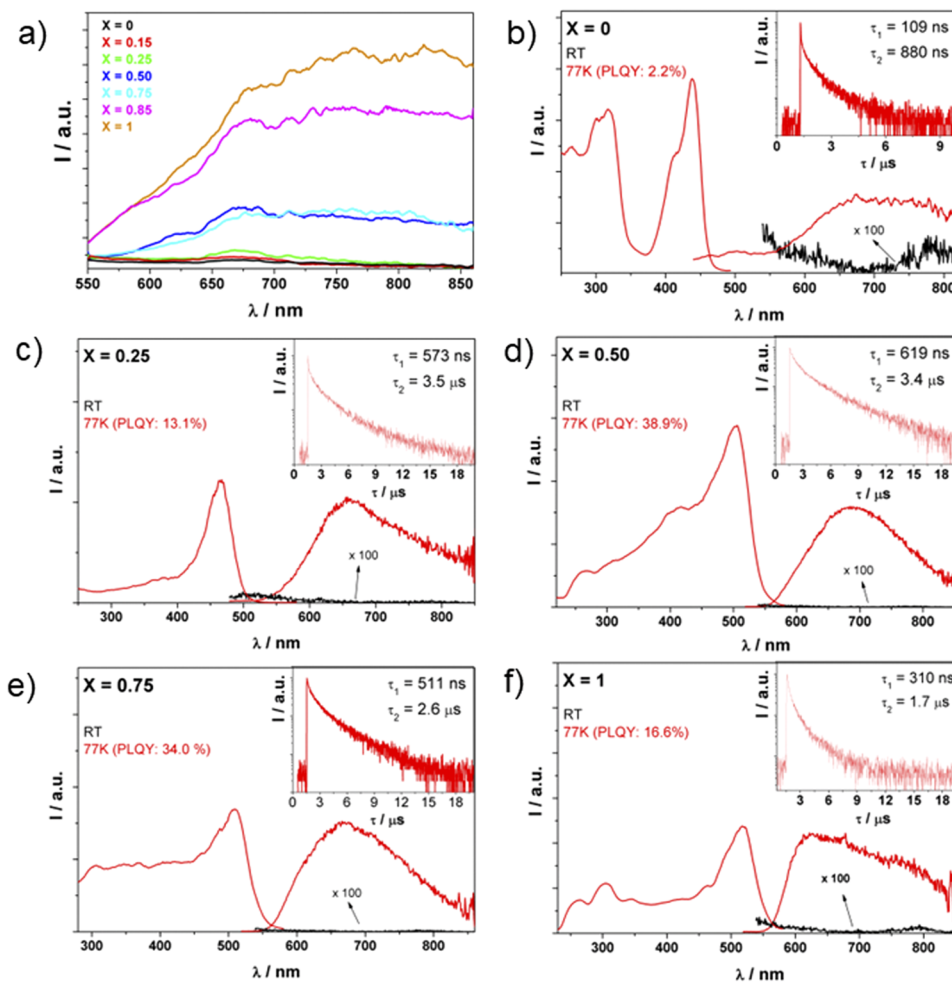
FIG. 3. (a) RT PL data for the $DA_2Ge(Br_{1-x}I_x)_4$ system. (b)–(f) Right: Comparison between the RT and LT (77 K) PL data for the samples of the $DA_2Ge(Br_{1-x}I_x)_4$ system with $x = 0$, 0.25, 0.5, 0.75, and 1 (inset: TRPL). Left: excitation spectra of $DA_2Ge(Br_{1-x}I_x)_4$ system obtained at LT.

for the previous samples, the patterns are dominated by the (00*l*), and the two reflections shown in Fig. 5 correspond to the (004) and (006) peaks of the orthorhombic symmetry providing information on the *c*-axis trend. Within each series, it is possible to observe a very slight shift of the peaks toward higher angles (smaller *c*-axis) from Ge to Sn and to Pb, which is opposite to the trend of the ionic radii, witnessing a possible reduction of octahedral distortion, particularly in the out of plane direction, as previously observed in other low-dimensional perovskites.[1,16,18] On the other hand, as also observed earlier, all the iodide compositions have a shorter *c*-axis, a trend due to the change of organic spacer staggering, which is in turn related to

the hydrogen bonding of the protonated ammonium to the halide, showing strong reduction of this distance when moving from iodide to bromide.[18,21–23]

The corresponding absorption measurements for the two series of samples at RT are reported in Figs. 5(b) and 5(c).

Replacing Ge for Sn results in a significant red-shift of the absorption, while the substitution for Pb leads to a clear blue-shift for both series and, as expected, moving from Br to I red-shifts all the curves of about 0.5 eV. The values of the experimental bandgaps, calculated from the Tauc plots, are the following: $DA_2SnBr_4 = 2.54$ eV, $DA_2GeBr_4 = 2.74$ eV, $DA_2PbBr_4 = 3.04$ eV, $DA_2SnI_4 = 1.87$ eV,
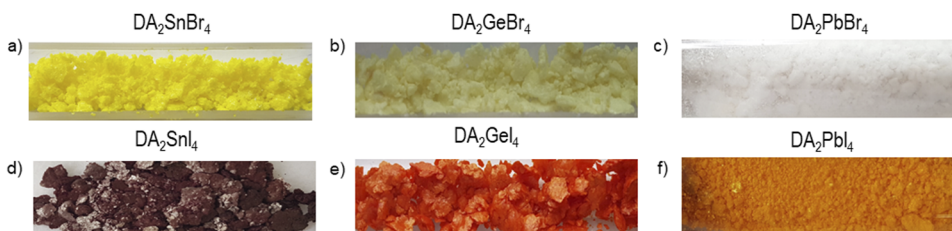

FIG. 4. Pictures of the (a) DA_2SnBr_4, (b) DA_2GeBr_4, (c) DA_2PbBr_4, (d) DA_2SnI_4, (e) DA_2GeI_4, and (f) DA_2PbI_4 samples.
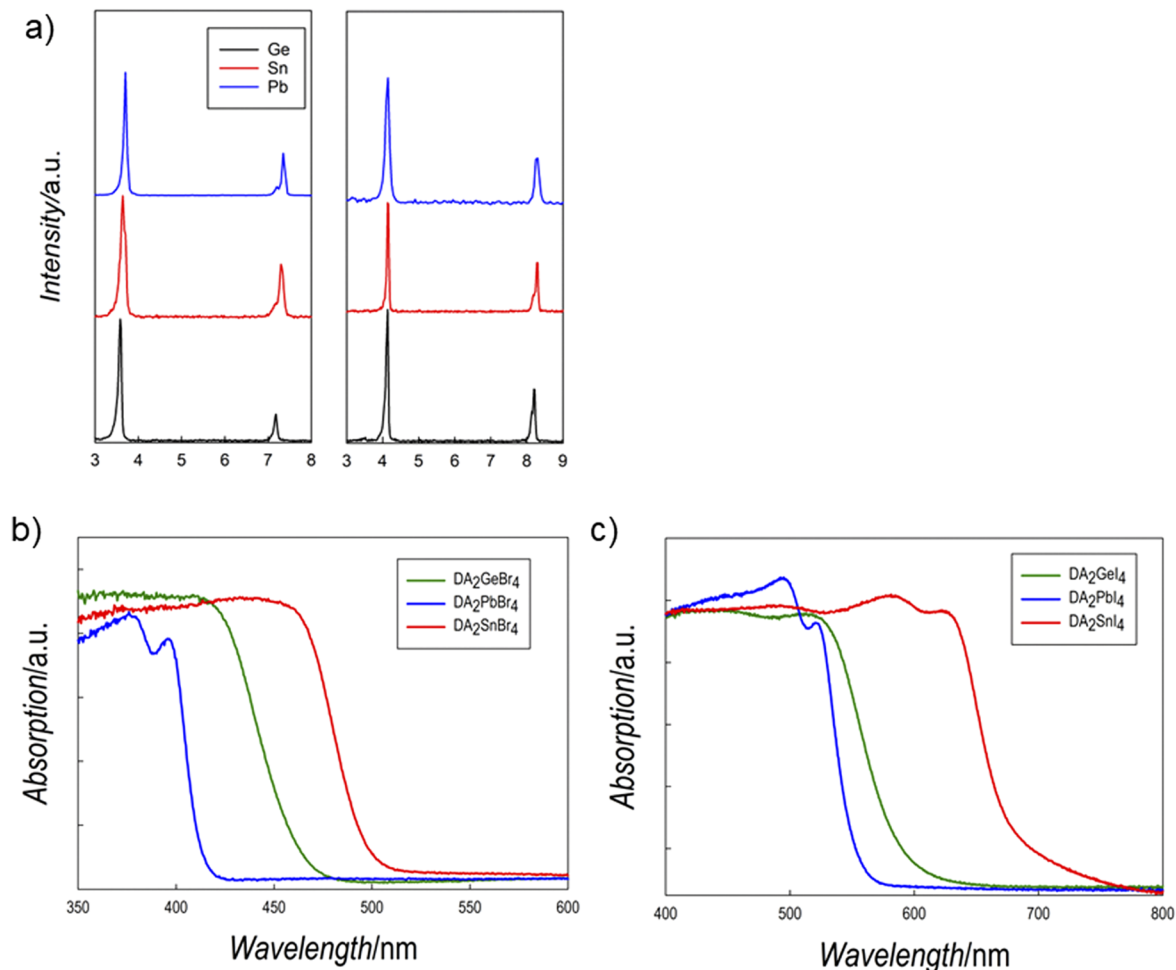
FIG. 5. (a) XRD patterns for DA_2SnBr_4, DA_2GeBr_4, DA_2PbBr_4, DA_2SnI_4, DA_2GeI_4, and DA_2PbI_4 samples. (b) UV-vis absorption measurements for DA_2SnBr_4, DA_2GeBr_4, and DA_2PbBr_4 and (c) for DA_2SnI_4, DA_2GeI_4, and DA_2PbI_4.

DA_2GeI_4 = 2.17 eV, and DA_2PbI_4 = 2.29 eV. As can be appreciated, within these two series of decylammonium-based 2D perovskites, by playing with the central atom and the halide, it is possible to modulate the absorption from the blue to the red region of the visible spectrum.

Figure 6 reports the RT PL spectra of the Sn and Pb containing samples and, for the sake of comparison, it also includes the spectra of DA_2GeI_4 already reported in Fig. 3(a).

DA_2SnBr_4 does not emit at RT, while the other three perovskites show PL spectra with very different characteristics compared to Ge-based compounds. The PL spectra of DA_2PbBr_4 and DA_2PbI_4 are very narrow if compared to Ge-based compounds, while DA_2SnI_4 lays somehow in between with a structure and reasonably wide emission. The PL spectra of lead and tin containing specimens well reflect the absorption features, as they show a structured emission involving two main contributions for the lead containing samples and three components for the tin one.[19,24] The structuring of the lead based 2D MHPs emission in two main

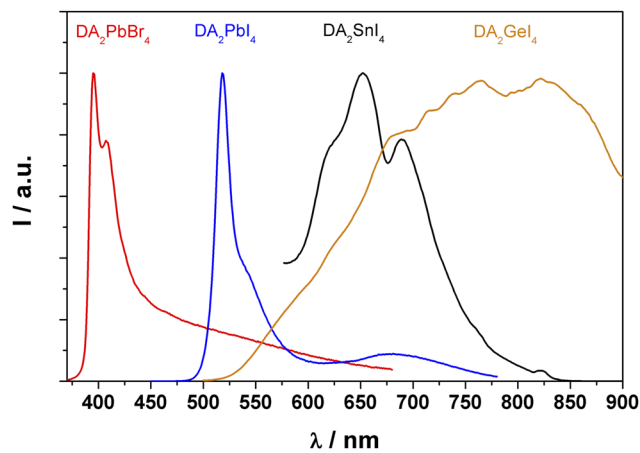FIG. 6. RT PL of DA_2PbBr_4, DA_2SnI_4, DA_2PbI_4, and DA_2GeI_4.
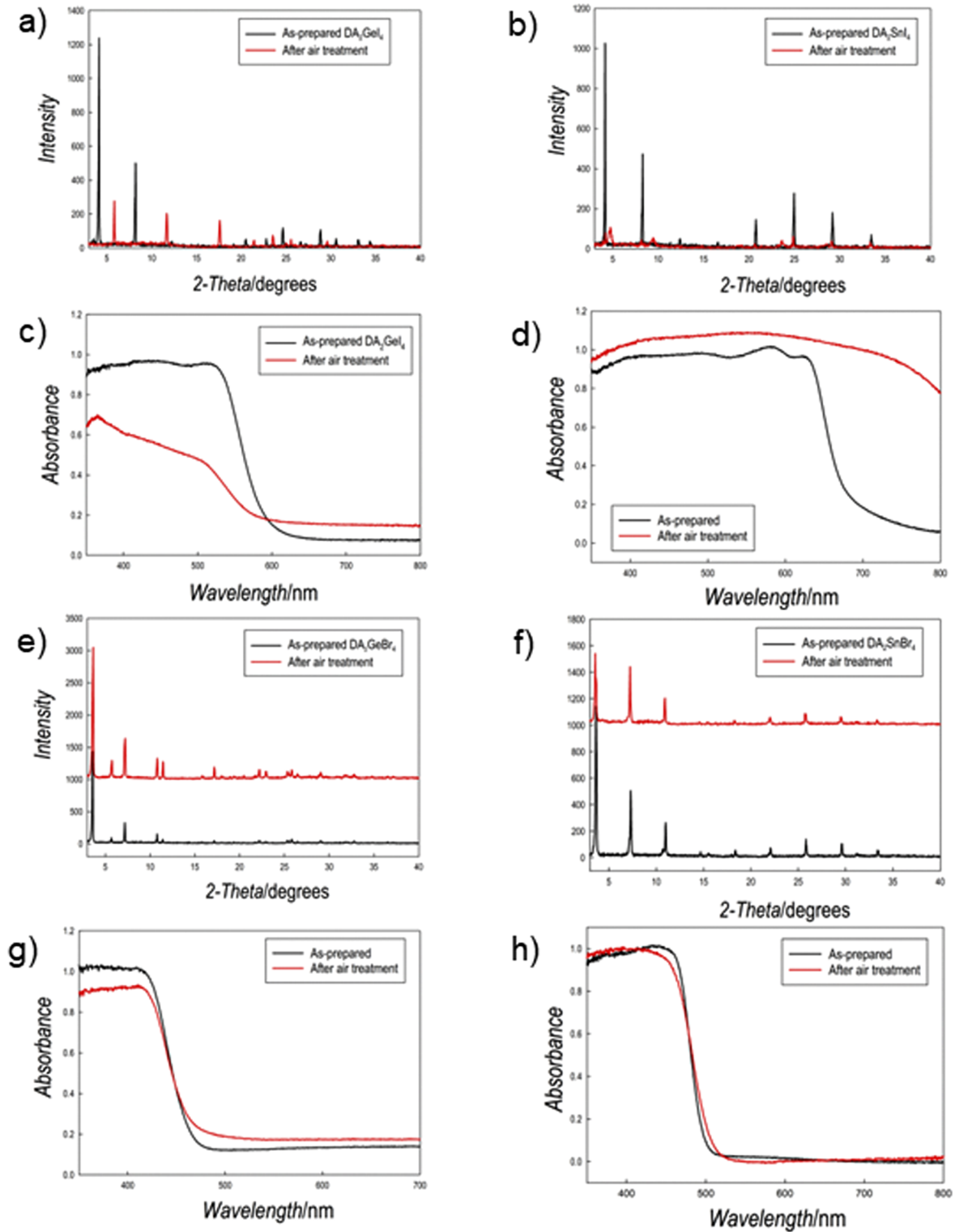
FIG. 7. XRD and UV-vis absorption data for as prepared and air-exposed samples of DA_2GeI_4 (a) and (c); DA_2SnI_4 (b) and (d); DA_2GeBr_4 (e) and (g); and DA_2SnBr_4 (f) and (h).

contributions (S1 and S2) has been attributed to phonon replica of the main line.[24] In tin based samples, this band structuring could be further modified by the contribution from trap states, which will be eventually dominant for Ge based compounds, *vide infra*. RT decays are very fast in all the compounds measured although the tin-based sample show also a long living minority contribution (see Fig. S3).

A general trend in the emission properties emerges from the comparison of different metal centered 2D perovskites. Narrow and intense PL associate with lead-based samples, this emission broads when moving to tin-based compounds, and finally it became very broad and weak for germanium-based samples. In these cases, we expect a high exciton–phonon scattering induced by the presence of long alkyl–ammonium chain. In addition, the exciton–phonon Fröhlich interaction of the 2D Sn-based perovskites was found to be one order of magnitude larger in tin perovskites in comparison to lead perovskites that can be at the origin of the increase in the FWHM of PL and to the more likely formation of self-trapped exciton states.[19] It is evident here that, for germanium-containing samples, this interaction would be even higher determining the conditions for a weak and broad room temperature emission, which only recovers a high intensity at 77 K.

A further characterization, which has been carried out on the present samples, is related to the assessment of their air-stability. It is known that 2D perovskites are, in general, more resistant to ambient conditions with respect to 3D perovskites due to the highly hydrophobic characteristics of the organic spacer.[1] On the other hand, when tin or germanium is present, the easy oxidation of these elements from +2 to +4 may also occur in low-dimensional perovskites. We afforded since some time a through engineering of stable lead-free perovskites trying to provide more environment resistant samples.[5,6,25,26] In this respect, we report here the structural and optical results obtained by exposing the samples for one month to laboratory air [relative humidity (RH) around 45%]. Figures 7(a)–7(h) report the XRD patterns and the absorption spectra for the as-prepared DA_2GeI_4, DA_2SnI_4, DA_2GeBr_4, and DA_2SnBr_4 samples and the corresponding measurements after air exposure for one month.

The data clearly demonstrate that iodide-based samples undergo an extended degradation as demonstrated by the XRD patterns showing the appearance of different diffraction patterns (which, at present, cannot be assigned to any known phase). Such structural change is also confirmed by the marked variation of the spectroscopic data [Figs. 3(c) and 3(d)]. On the other hand, it is very interesting to observe the impressive stability of the corresponding bromide samples. After one month of air exposure, both the XRD data and the UV-vis absorption spectroscopy measurements are practically unchanged. This result confirms some previous evidences provided by our group highlighting the possible role of very thin surface passivation (and protective) oxide layers on Sn- and Ge-containing perovskites as well as the superior stability of bromide-based MHPs due to the lower ionic character of this halide with respect to iodide.[14,16,18]

CONCLUSIONS

In the present paper, we reported a series of novel 2D perovskites, including decylammonium as organic spacer. Novel

Ge- and Sn-based bromide and iodide materials are reported and investigated for the first time. $DA_2Ge(Br_{1-x}I_x)_4$ system shows a strong correlation between structural and optical properties, with two distinct regimes with a step reduction of *c*-axis and bandgap from $x = 0$ to $x = 0.5$ followed by a plateau in both data up to $x = 1$. RT PL data show a progressive intensity increase and peak narrowing with the increase of the iodide content, with mixed compositions showing the highest QYs. The role of central metal has been investigated by replacing Ge with Pb and Sn for bromide and iodide compounds. The presence of tin red-shifts the absorbance of the samples, opposite to the blue shift induced by Pb. On the other hand, a progressive PL broadening is clear by moving from Pb to Sn and to Ge, possibly related to the increased structural distortions and exciton–phonon Fröhlich interactions. Finally, the air stability of Sn- and Ge-containing samples has been verified by collecting data after laboratory air exposure, confirming a trend of increased stability with the increase of the anion hardness.

To conclude, the series of novel 2D perovskites presented in this work widen our actual knowledge of structure–property correlations in lead and lead-free systems. In addition, by keeping the same organic spacer (decylammonium), the tuning of central metal and halide allowed to modulate the absorption in the whole visible spectrum and to provide samples with narrow and broad emissions with, in some cases, appreciable quantum yields that can be nicely modulated through halide alloying, a strategy of potential exploitation in other low-dimensional perovskites. The systems presented in this work are clearly of interest in many possible applicative fields, also considering the superior stability of lead-free bromide compounds, and are worth of being further investigated from an experimental and theoretical perspective.

SUPPLEMENTARY MATERIAL

See the supplementary material for experimental details, Tauc plots, and additional PL measurements.

AUTHOR DECLARATIONS

Conflict of Interest

The authors have no conflicts to disclose.

Author Contributions

Rossella Chiara: Investigation (equal). **Gianluca Accorsi**: Data curation (lead); Formal analysis (equal); Writing – original draft (supporting). **Andrea Listorti**: Data curation (equal); Formal analysis (equal); Writing – original draft (equal). **Mauro Coduri**: Data curation (equal). **Clarissa Coccia**: Data curation (equal). **Costanza Tedesco**: Data curation (equal). **Marta Morana**: Data curation

(equal); Formal analysis (equal); Writing – original draft (supporting). **Lorenzo Malavasi**: Conceptualization (lead); Supervision (lead); Writing – original draft (lead).

DATA AVAILABILITY

The data that support the findings of this study are available within the article and its supplementary material.

REFERENCES

[1] X. Li, J. M. Hoffman, and M. G. Kanatzidis, Chem. Rev. **121**, 2230 (2021).

[2] R. Dong, C. Lan, F. Li, S. Yip, and J. C. Ho, Nanoscale Horiz. **4**, 1342 (2019).

[3] C. Fang, H. Wang, Z. Shen, H. Shen, S. Wang, J. Ma, J. Wang, H. Luo, and D. Li, ACS Appl. Mater. Interfaces **11**, 8419 (2019).

[4] A. Krishna, S. Gottis, M. K. Nazeeruddin, and F. Sauvage, Adv. Funct. Mater. **29**, 1806482 (2019).

[5] L. Romani, A. Bala, V. Kumar, A. Speltini, A. Milella, F. Fracassi, A. Listorti, A. Profumo, and L. Malavasi, J. Mater. Chem. C **8**, 9189 (2020).

[6] L. Romani, A. Speltini, R. Chiara, M. Morana, C. Coccia, C. Tedesco, V. Armenise, S. Colella, A. Milella, A. Listorti, A. Profumo, F. Ambrosio, E. Mosconi, R. Pau, F. Pitzalis, A. Simbula, D. Ricciarelli, M. Saba, M. Medina-Llamas, F. De Angelis, and L. Malavasi, Cell Rep. Phys. Sci. **4**, 101214 (2023).

[7] E. I. Marchenko, S. A. Fateev, A. A. Petrov, V. V. Korolev, A. Mitrofanov, A. V. Petrov, E. A. Goodilin, and A. B. Tarasov, Chem. Mater. **32**, 7383 (2020).

[8] A. Abate, Joule **1**, 659 (2017).

[9] J. Li, H.-L. Cao, W.-B. Jiao, Q. Wang, M. Wei, I. Cantone, J. Lü, and A. Abate, Nat. Commun. **11**, 310 (2020).

[10] C. Ponti, G. Nasti, D. Di Girolamo, I. Cantone, F. A. Alharthi, and A. Abate, Trends Ecol. Evol. **37**, 281 (2022).

[11] X. Chang, D. Marongiu, V. Sarritzu, N. Sestu, Q. Wang, S. Lai, A. Mattoni, A. Filippetti, F. Congiu, A. G. Lehmann, F. Quochi, M. Saba, A. Mura, and G. Bongiovanni, Adv. Funct. Mater. **29**, 1903528 (2019).

[12] L.-J. Chen, RSC Adv. **8**, 18396 (2018).

[13] M.-G. Ju, J. Dai, L. Ma, and X. C. Zeng, J. Am. Chem. Soc. **139**, 8038 (2017).

[14] R. Chiara, M. Morana, and L. Malavas, ChemPlusChem **86**, 879 (2021).

[15] D. Yang, G. Zhang, R. Lai, Y. Cheng, Y. Lian, M. Rao, D. Huo, D. Lan, B. Zhao, and D. Di, Nat. Commun. **12**, 4295 (2021).

[16] R. Chiara, M. Morana, M. Boiocchi, M. Coduri, M. Striccoli, F. Fracassi, A. Listorti, A. Mahata, P. Quadrelli, M. Gaboardi, C. Milanese, L. Bindi, F. De Angelis, and L. Malavasi, J. Mater. Chem. C **9**, 9899 (2021).

[17] M. Morana, R. Chiara, B. Joseph, T. B. Shiell, T. A. Strobel, M. Coduri, G. Accorsi, A. Tuissi, A. Simbula, F. Pitzalis, A. Mura, G. Bongiovanni, and L. Malavasi, iScience **25**, 104057 (2022).

[18] A. Pisanu, M. Coduri, M. Morana, Y. O. Ciftci, A. Rizzo, A. Listorti, M. Gaboardi, L. Bindi, V. I. E. Queloz, C. Milanese, G. Grancini, and L. Malavasi, J. Mater. Chem. A **8**, 1875 (2020).

[19] T. Zhang, C. Zhou, X. Feng, N. Dong, H. Chen, X. Chen, L. Zhang, J. Lin, and J. Wang, Nat. Commun. **13**, 60 (2022).

[20] A. Lemmerer and D. G. Billing, Dalton Trans. **41**, 1146 (2012).

[21] K. L. Svane, A. C. Forse, C. P. Grey, G. Kieslich, A. K. Cheetham, A. Walsh, and K. T. Butler, J. Phys. Chem. Lett. **8**, 6154 (2017).

[22] A. Bernasconi, K. Page, Z. Dai, L. Z. Tan, A. M. Rappe, and L. Malavasi, J. Phys. Chem. C **122**, 28265 (2018).

[23] J. H. Lee, J.-H. Lee, E.-H. Kong, and H. M. Jang, Sci. Rep. **6**, 21687 (2016).

[24] K. Gauthron, J.-S. Lauret, L. Doyennette, G. Lanty, A. Al Choueiry, S. J. Zhang, A. Brehier, L. Largeau, O. Mauguin, J. Bloch, and E. Deleporte, Opt. Express **18**, 5912 (2010).

[25] L. Romani, A. Speltini, F. Ambrosio, E. Mosconi, A. Profumo, M. Marelli, S. Margadonna, A. Milella, F. Fracassi, A. Listorti, F. De Angelis, and L. Malavasi, Angew. Chem., Int. Ed. **60**, 3611 (2021).

[26] A. Pisanu, A. Speltini, P. Quadrelli, G. Drera, L. Sangaletti, and L. Malavasi, J. Mater. Chem. C **7**, 7020 (2019).

28 June 2023 08:33:29